Cell, Vol. 119, 47–60, October 1, 2004, Copyright ©2004 by Cell Press

Mechanisms of Conformational Change for a Replicative Hexameric Helicase of SV40 Large Tumor Antigen

Dahai Gai,[1,2] Rui Zhao,[1] Dawei Li,[1,3]
Carla V. Finkielstein,[1] and Xiaojiang S. Chen[1,2,*]
[1]Department of Biochemistry and Molecular Genetics
University of Colorado Health Sciences Center
Denver, Colorado 80262
[2]Department of Molecular and Computational Biology
University of Southern California
Los Angeles, California 90089

Summary

The large tumor antigen (LTag) of simian virus 40, an AAA$^+$ protein, is a hexameric helicase essential for viral DNA replication in eukaryotic cells. LTag functions as an efficient molecular machine powered by ATP binding and hydrolysis for origin DNA melting and replication fork unwinding. To understand how ATP binding and hydrolysis are coupled to conformational changes, we have determined high-resolution structures (~1.9 Å) of LTag hexamers in distinct nucleotide binding states. The structural differences of LTag in various nucleotide states detail the molecular mechanisms of conformational changes triggered by ATP binding/hydrolysis and reveal a potential mechanism of concerted nucleotide binding and hydrolysis. During these conformational changes, the angles and orientations between domains of a monomer alter, creating an "iris"-like motion in the hexamer. Additionally, six unique β hairpins on the channel surface move longitudinally along the central channel, possibly serving as a motor for pulling DNA into the LTag double hexamer for unwinding.

Introduction

The oncogenic large tumor antigen (LTag) encoded by simian virus 40 (SV40) (Sullivan and Pipas, 2002) is essential for initiation and elongation of viral DNA replication (Borowiec et al., 1990; Stillman et al., 1985). LTag melts the DNA at the origin of replication and unwinds the replication forks (Dean et al., 1987; Stillman, 1994). In this regard, it is a functional homolog of the minichromosome maintenance (MCM) protein, a putative replicative helicase in eukaryotic and archaeal cells (Chong et al., 2000; Fletcher et al., 2003; Kelman et al., 1999).

LTag (708 residues) has three major functional domains: a DnaJ homology domain (DnaJ, residues 1–82) (Campbell et al., 1997), an origin DNA binding domain (OBD, residues 131–259) (Arthur et al., 1988) (reviewed in Simmons [2000]), and a helicase domain (res. 251–627) (Li et al., 2003). The DnaJ domain participates in remodeling protein complexes and is dispensable for in vitro DNA replication. The OBD recognizes the viral origin of replication (Arthur et al., 1988), which is required for the recruitment of LTag to the origin for DNA replication.

To initiate replication, LTag first assembles at the origin as a double hexamer that distorts and melts the double-stranded origin DNA (Borowiec et al., 1991; Bullock et al., 1991; Gomez-Lorenzo et al., 2003). The LTag double hexamer then recruits replication protein A, topoisomerase I, and polymerase-α/primase to form a replication initiation complex (Brush et al., 1995; Tsurimoto and Stillman, 1991). During elongation stage, the LTag double hexamer acts as a helicase to unwind the two replication forks bidirectionally (Borowiec et al., 1991; Bullock, 1997; Smelkova and Borowiec, 1998). Indeed, by addition of purified replication proteins and LTag to SV40 origin-containing DNA, a eukaryotic replication system can be reconstituted in vitro (Stillman and Gluzman, 1985; Tsurimoto and Stillman, 1991; Waga and Stillman, 1994; Wobbe et al., 1987).

The hexameric structure of LTag helicase domain (residues 251–627) in a nucleotide (Nt)-free form has been reported previously (Figures 1A and 1B) (Li et al., 2003). Based on the structure, as well as on previous biochemical studies (Borowiec et al., 1990; Fanning and Knippers, 1992; Wessel et al., 1992), an iris model has been proposed for a LTag double hexamer to melt the origin and unwind the dsDNA. Additionally, a looping model has been proposed for the bidirectional unwinding of the two replication forks by a double-hexameric replicative helicase in the eukaryotic replication system (Li et al., 2003). The monomer of the LTag helicase has three structural domains (termed D1, D2, and D3, Figure 1A). The D2 domain is a typical AAA$^+$ domain that binds ATP. Members of AAA$^+$ family are involved in diverse cellular processes, such as DNA replication, membrane fusion, and protein degradation (Neuwald et al., 1999) (Ogura and Wilkinson, 2001). One common feature of AAA$^+$ proteins is their ability to couple the energy of ATP binding and hydrolysis to conformational changes that are used for the remodeling of their targets. Understanding the mechanism by which ATP binding and hydrolysis drive conformational changes in hexameric helicases and other AAA$^+$ proteins is hindered by the lack of high-resolution structural data for a given member in different Nt binding states.

In this report, we describe two conclusions derived from a set of high-resolution structures of the LTag hexamers in distinct conformations, corresponding to different Nt binding states. The first is the detailed molecular mechanisms of conformational changes triggered by ATP binding and hydrolysis, and the second is evidence for an all-or-none (concerted) Nt binding mode and for a concerted ATP binding and hydrolysis mechanism by a hexameric molecular machine. In addition, we propose a mechanism for coupling the energy of ATP binding and hydrolysis to the unwinding of DNA by LTag. The mechanistic states of LTag described here have general implications for other hexameric helicases and AAA$^+$ molecular machines.

*Correspondence: xiaojiang.chen@usc.edu
[3]Present address: National Laboratory, China Agricultural University, Beijing 10049, China.

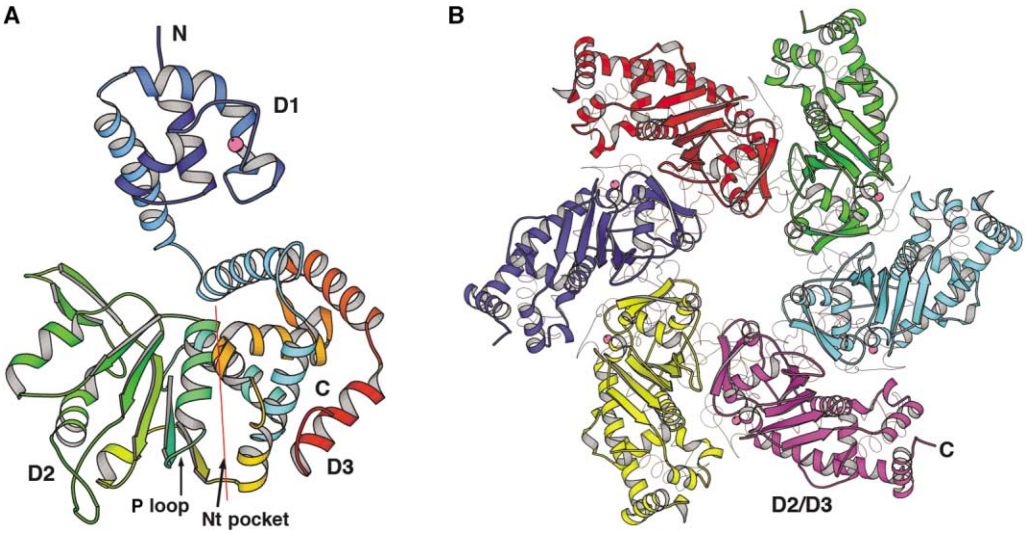

Figure 1. An Overview of the Nt-Free Structure of a LTag Monomer and its Hexamer

(A) The LTag domain structure in ribbon diagram. D1 is the N-terminal domain, D2 the AAA+ domain, and D3 the C-terminal α-helical domain. The thin red line shows the border between D2 and D3. The N and C termini are labeled as N and C. ATP binding P loop and the Nt binding pocket (Nt pocket) for binding the base are indicated by arrows.

(B) The C-terminal view of a LTag hexamer structure along the hexameric axis, with the D2/D3 on top.

Results

Hexameric Structures of Different Nt Binding States

In order to understand the mechanism of conformational changes triggered by ATP binding and hydrolysis, we determined a set of high-resolution structures of LTag helicase domain (residues 251–627) in different Nt binding states. These structures include the ATP bound (and ADP-BeF_3^- bound), ADP bound, and the Nt-free states of the hexameric LTag protein.

The first ATP bound structure was determined from a cocrystal of LTag with ATP in the absence of Mg^{2+} ion, a condition not supporting ATP hydrolysis. Despite the relatively low resolution at 3.42 Å, a Fourier difference synthesis revealed electron density clearly corresponding to ATP at the Nt binding pocket (see Supplemental Figure S1 at http://www.cell.com/cgi/content/full/119/1/47/DC1/). A higher-resolution structure (1.94 Å, Table 1) containing the ATP analog ADP-BeF_3^- was also determined from a crystal soaked with BeF_3^- plus either ATP+Mg^{2+} or ADP+Mg^{2+}. BeF_3^- is a phosphoryl mimic, which has been used in combination with ADP to form ADP-BeF_3^-, a nonhydrolyzable ATP analog (Fisher et al., 1995; Levin et al., 2003; Petsko, 2000). Not surprisingly, the overall structure with ADP-BeF_3^- (Figure 2A) is very similar to the structure of the ATP bound structure: the Cα backbone of the two structures can be superimposed with a rmsd of 0.581 (see Supplemental Figure S2 on the *Cell* web site).

The ADP bound structure (to 1.96 Å, Figure 2B) was determined from a crystal form obtained by cocrystallizing LTag with ATP+$MgSO_4$, a condition supporting ATP hydrolysis. The same ADP bound structure was also obtained by cocrystallizing LTag with ADP+$MgSO_4$. The Nt-free structure at 2.6 Å resolution was determined from a crystal obtained in the absence of ATP/ADP. This structure is similar to but has a higher resolution than the previously reported Nt-free structure (Li et al., 2003).

From Figure 2, it is apparent that the three structural states (ATP bound, ADP bound, and Nt-free) of LTag hexamers have significant conformational differences (Figures 2A–2C). The differences are most apparent in the size/shape of the central channel and the monomer-monomer interfaces in a hexamer (Figures 2A–2C). The ATP bound form has the smallest channel opening (Figure 2A), with a distance of approximately 14 Å between backbone atoms at the narrowest point. Much larger openings exist in the channel right next to the narrowest point, with dimensions as wide as 47 Å. These structural features of the ATP bound form are essentially the same as the ADP-BeF_3^- bound structure. In this regard, the

Table 1. Summary of Crystallographic Data and Refinement Statistics

Space Group	$P2_1$	C2	P321
Data Analysis			
Resolution (Å)	30.0–1.94	30.0–1.96	30.0–2.60
Observations	3,141,371	711,416	369,508
Unique Reflections	231,936	112,603	18,058
Completeness (%)	98.1	99.3	95.2
R_{sym} (%)	6.6	5.1	7.7
I/s	20.4	24.1	25.0
Molecules/asu	6	3	2
Refinement Statistics			
R_{work} (%)	21.98	23.63	23.25
R_{free} (%)	24.40	26.41	27.09
Total Protein Atoms	17,606	8,802	5,866
Total Water	806	230	187
RMS Deviation			
Bonds (Å)	0.008	0.010	0.011
Angles (°)	1.286	1.305	1.331

$R_{sym} = \Sigma_{ij}|Ii(j) - <I(j)>|/\Sigma_{ij} I_i(j)$, where $I_i(j)$ is the ith measurement of reflection j, and $<I(j)>$ is the overall weighted mean of i measurements. $R_{work} = \Sigma|F_o - F_c|/\Sigma F_o$, where F_o and F_c are the observed and calculated structure factors, respectively. R_{free} is calculated the same way as R_{work}, except that the F_o used for R_{free} calculation was the 5% of reflections not used in the refinement.

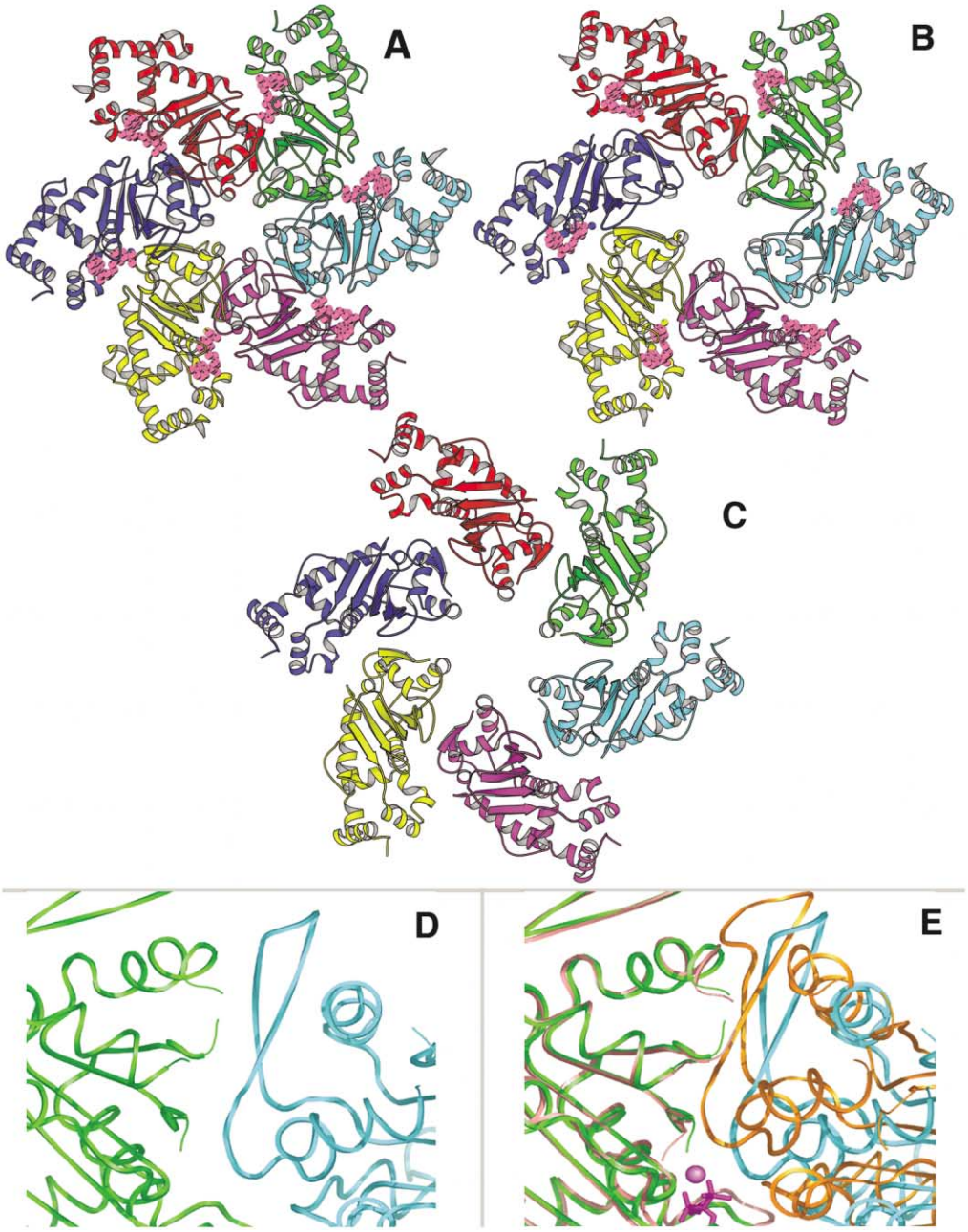

Figure 2. The Changes of Channel Openings and Hexamerization Interfaces of LTag Hexamers in Three Nt Binding States, Viewing from the C-Terminal End

To provide a clearer view of the Nt binding cleft at the hexamerization interface, only the D2/D3 parts of the hexamer are shown. Each of the six monomers is in a different color. (A) The ATP bound hexamer structure. The six ATPs at the cleft between two monomers are in pink. (B) The ADP bound hexamer structure, showing ADP (pink) at the cleft. (C) The Nt-free hexamer structure. (D) A close-up view of the cleft between two neighboring monomers (in green and cyan) of the Nt-free structure. (E) The same view of the cleft between two neighbors from two different Nt bound structures: the Nt-free structure (in green and cyan) and the ATP bound structure (in pink and gold), showing a narrowing of the cleft when ATP is bound. The bound ATP and Mg^{2+} are in purple.

ADP-BeF_3^- bound structure can be considered as the ATP bound structure.

In the ADP bound form, the channel has an obvious asymmetrical shape with approximately 17 Å and 20 Å between backbone atoms in two directions (Figure 2B). The Nt-free structure has the widest opening, approximately 22 Å between backbone atoms (Figure 2C). A side channel (on the side wall of a LTag hexamer), which has been postulated to serve as an exit for ssDNA in a looping model (Li et al., 2003), has similar dimensions in all three Nt binding states, despite the dramatic changes in the central channel openings.

The change of hexamer channel size and shape is reflected by the change of monomer-monomer interface in the respective hexamers, where the relative orientation and distance between two neighbors change in

different Nt states (Figures 2D and 2E). ATP binding leads to narrowing of the cleft between two monomers (Figure 2E), dramatically increasing the buried surface area at the interface. The average buried surface area between two monomers in the ATP bound hexamer is ~4344 Å^2, in ADP bound hexamer is ~3198 Å^2, and in the Nt-free hexamer drops to 2474 Å^2.

Change of Domain Angles and Orientations within a Monomer

The structural changes in a hexamer are correlated with the conformational changes in individual monomers. To identify the conformational changes in response to Nt binding, the monomer structures of various Nt binding states are overlapped (Figure 3). ATP binding results in a narrowing of the angle between D1 and D2/D3 by ~25° (Figure 3B, green and pink), accompanied by an ~16° twist (Figure 3E). These motions pivot around helix H5. In the ADP bound hexamer, there are two very different conformations (yellow and purple in Figure 3C), both with intermediate domain angles and orientations between those of the Nt-free (green) and of the ATP bound structures (pink). The domain angles of the two distinct ADP bound conformations are approximately 15° and 8° narrower than the Nt-free state (green) (Figure 3C), and the twist angles are approximately 8° and 4° compared with the Nt-free state (Figure 3F only shows the conformation in yellow for clarity).

A Novel Nt Binding Mode in LTag Hexamer

In both the ATP and ADP bound structures, Fourier difference calculations using the refined models show clear electron density for ATP+Mg^{2+} (or ADP-BeF_3^-+Mg^{2+}, Figure 4A) and ADP+Mg^{2+} (Figure 4B) in all monomers. The density was obtained before ATP or ADP was built. Both density maps reveal the hexaliganded coordination of Mg^{2+}. One of the six ligands for Mg^{2+} is from the γ-phosphate (γ-Pi) oxygen in the ATP structure (Figure 4A), while a water molecule (W2) occupies the γ-Pi position in the ADP structure (Figure 4B). Since the ATP analog structure was obtained by soaking ADP containing crystals in BeF_3^- plus either ADP+Mg^{2+} or ATP+Mg^{2+}, the ATP density in Figure 4A should correspond to ADP-BeF_3^-. Because the overall structures of the ATP bound (at 3.42 Å resolution) and the ADP-BeF_3^- bound form are very similar (Supplemental Figure S2) and also because ADP-BeF_3^- is a ground state analog of ATP, ADP-BeF_3^- will be referred to as ATP in the following description.

Several lines of evidence suggest that the density in the Fourier difference map is ATP and not a mixture of ATP and ADP. First, even though one asymmetric unit contains a complete hexamer in this structure, each monomer is treated differently, and no noncrystallographic symmetry (NCS) averaging was used in the structural determination and refinement. Yet, the Fourier difference map before building ATP+Mg^{2+} atoms shows clear ATP+Mg^{2+} densities (Figure 4A), which are essentially identical in each monomer. Second, after building the ATP+Mg^{2+} into the model and subsequent refinement, the γ-Pi of all six ATPs have only slightly higher B factors than the β-Pi and α-Pi. Third, an occupancy refinement for the bound ATP yielded values around 1.0 (100%) for the ATP in each monomer. These observations indicate that all six ATP binding sites in a hexamer are fully occupied by ATP.

Likewise, the electron density maps for ADP+Mg^{2+} are essentially the same in every subunit of the ADP bound structure. However, because the ADP bound form has three different conformations, with two drastically different, an important consideration is whether each monomer indeed binds an ADP+Mg^{2+}. Again, because each site shows strong ADP+Mg^{2+} density in the Fourier difference map calculated from a model refined in the absence of ADP+Mg^{2+} without using NCS constraints/restraints, the ADP+Mg^{2+} likely exists in each monomer. Additionally, the B factors of the ADP+Mg^{2+} in each subunit refined without NCS restraints/constraints are essentially identical, and the occupancy refinement yields a value of about 1.0 for the ADP in each subunit, indicating again the full occupancy of all six sites. Because both ATP and ADP each have full occupancy in their respective structure, the Nt binding by a LTag hexamer is consistent with an all-or-none mode (or a concerted mode).

The Binding Pocket for Purine Base

In the ATP bound structure of SV40 LTag, the Nt triphosphate binds to the P loop, and its base inserts into a gap between D2 and the helical D3 of a monomer (Figure 4C; also see Figure 1A for orientation). However, interactions with the base in this gap are identical in both the ATP and ADP structures. Furthermore, the gap conformation stays essentially the same even in the absence of Nt, as shown by the good agreement of the overlaps of the three structures (ATP, ADP bound, and Nt-free) in Figure 4D, suggesting that the packing interactions with the base of ATP/ADP do not play a major role in directly triggering conformational changes. This is different from F1-ATPase, a hexameric machine. ATP binding plays a major role in closing a large gap (around 11 Å) around the base binding pocket (Abrahams et al., 1994) (Figure 4F), directly triggering the conformational change for F1-ATPase.

Interaction of *cis*-Residues with ATP

Unlike the Nt base that only interacts with residues from the same monomer (termed the "*cis*-monomer"), the phosphate and pentose moiety of ATP/ADP interact with both the *cis*-monomer and its immediate neighbor (termed the "*trans*-monomer"). For the interactions with the *cis*-monomer residues (*cis*-residues), the triphosphate rests across the P loop with the γ-Pi and β-Pi interacting with the Walker A residue K432 (Figure 4C). Two threonines (T433 and T434) of the P loop also bind the triphosphate: T433 coordinates an Mg^{2+} ion to interact with the γ-Pi and β-Pi, while T434 interacts directly with α-Pi. Additionally, two *cis*-residues outside the P loop, D474 of the Walker B motif and N529, interact with the γ-Pi directly through H bonds and indirectly via a water molecule (W1) that is positioned more or less apical to the γ-Pi.

Conservation of *cis*-Residue Conformations and ADP Release

The conformations of most *cis*-residues that bind ATP are conserved in the ADP and Nt-free structures (Figure

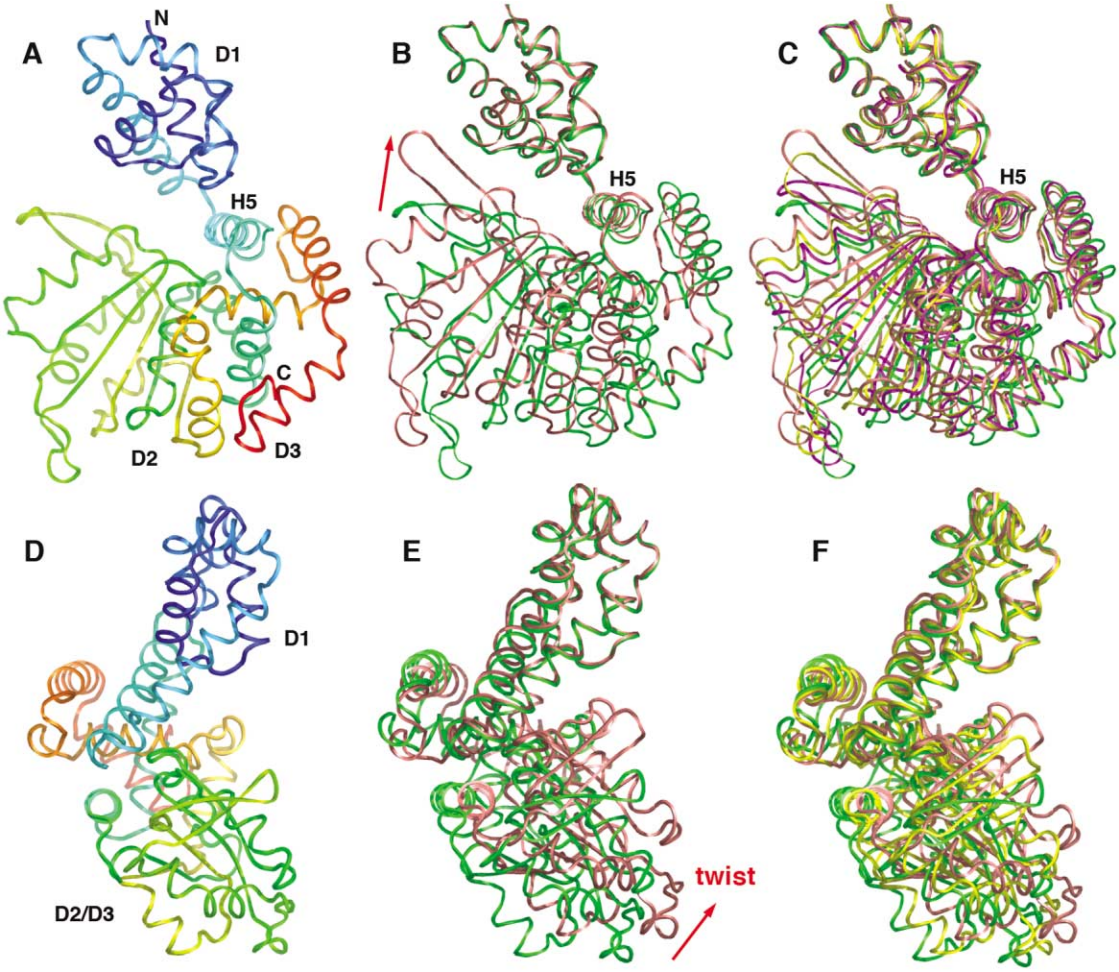

Figure 3. The Change of Domain Angles and Orientations in Different Nt Binding States

(A) The domain structure of a LTag monomer in the Nt-free state. The three domains, D1, D2, and D3, are labeled. H5 denotes α helix 5.
(B) The overlap of two monomers from the Nt-free structure (green) and ATP bound structure (pink), showing the narrowing between D1 and D2/D3. The overlap is based on D1.
(C) The overlap of four monomers that are from Nt-free (green), ATP bound (pink), and ADP bound (yellow and purple) structures. Note that the ADP bound structure has two structural states.
(D) The same Nt-free LTag monomer structure shown in (A) but viewed with a 120° rotation along the vertical axis.
(E) The same structures as in (B) but with a 120° rotation, showing the twist (or rotation, ~16°) of D2/D3 relative to D1 when ATP is bound.
(F) The same structures as in (C) but with a 120° rotation, showing the relative domain twist in three states. For clarity, the ADP conformation in purple is deleted.

4D), which is unexpected, considering the large conformational differences of the three Nt binding states. However, three of these *cis*-residues do adopt different conformations. One is the Walker B residue D474 (Figure 4D). The other two are T433 and I428 on the P loop (Figure 4E). T433 from both the ATP and ADP bound structures overlap exactly, but it shifts toward the β-Pi position in the empty state (yellow side chain) to generate steric clash if an ADP were bound. Compared with the ATP state (orange side chain), another residue I428 in the ADP state (purple) moves and rotates toward the center of the P loop where phosphate locates, which allows ADP but not ATP in the P loop. In the Nt-free structure, I428 (yellow) turns even further to sterically disallow the presence of ADP. Thus, the movement of I428 and T433 will both create steric clashes with the β-Pi of ADP (Figure 4E), which could serve to eject ADP as an ADP release mechanism.

Interactions of *trans*-Residues with ATP

Bordering the P loop of the *cis*-monomer is the *trans*-monomer that contributes five residues that interact with the ATP phosphate and ribose. These residues, referred to as *trans*-residues, include tK418, tK419, tR540, tD502, and tR498 ("t" for "*trans*-") (Figure 5A). Residue tR540 (magenta), located close to the end of the triphosphate, binds γ-Pi directly. Adjacent to tR540 is a negatively charged residue tD502 (orange), which interacts with tR540, possibly to stabilize the positively charged Arg side chain for efficient ATP hydrolysis. Residue tD502 also interacts with γ-Pi and β-Pi through a water molecule. Two other residues, tK418 (pink) and tK419

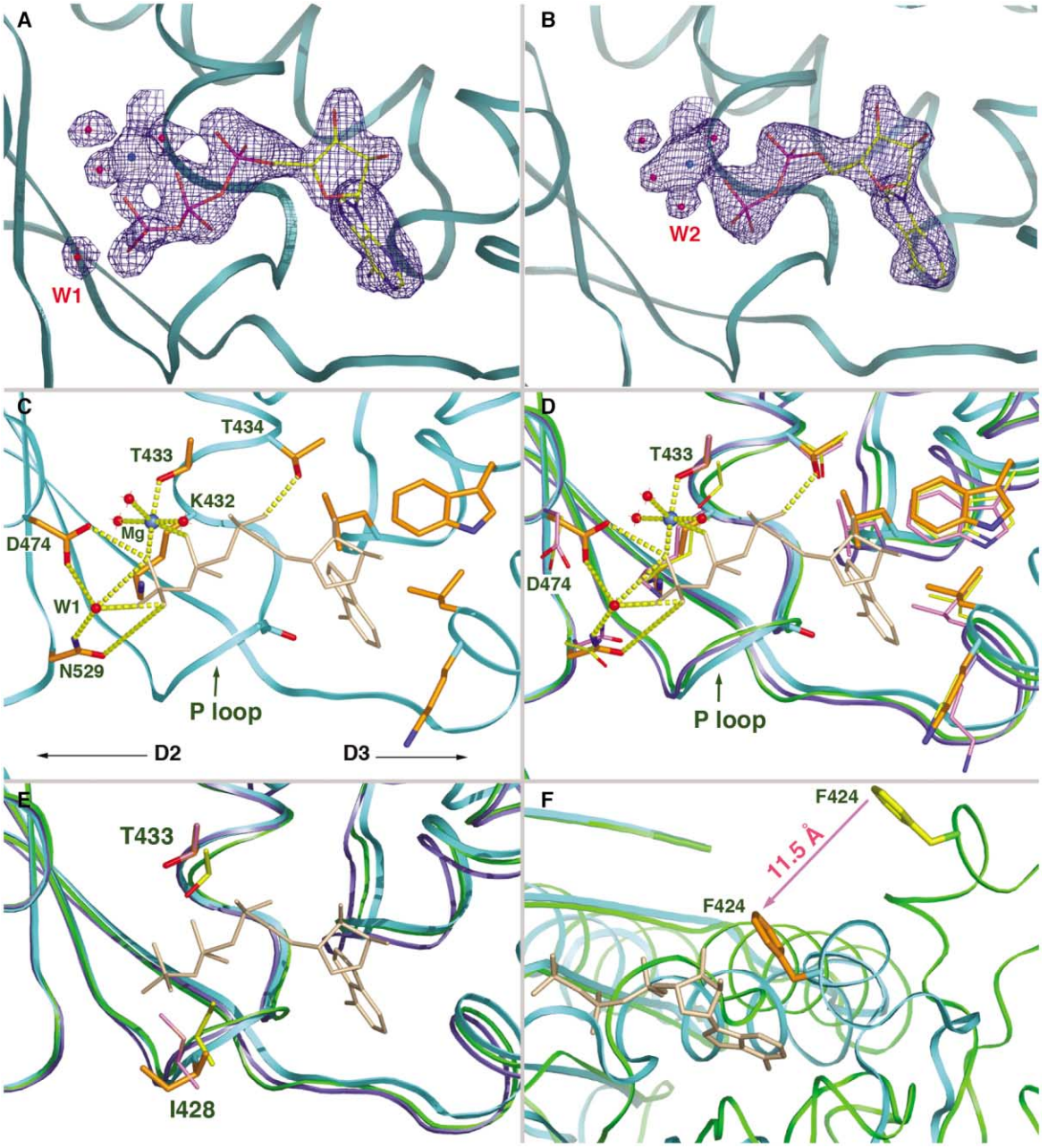

Figure 4. Conformation of the Nt Binding Pocket of the *cis*-Monomer

(A and B) The Fourier difference maps corresponding to ATP (1.94 Å) and ADP (1.96 Å), plotted at 2.3 σ level. The hexaliganded octahedron coordination of the Mg^{2+} ion is clearly seen in both maps. Red dots are water, and the blue dot is Mg^{2+} ion.

(C) The interactions of ATP (silver) with *cis*-residues around the Nt binding pocket. Dashed lines indicate bonding interactions.

(D) The overlap of LTag monomers from three Nt states, based on the superposition of the β sheet of D2. ATP (silver) is shown as a reference. The overlap shows that the pocket conformations are essentially the same for the ATP bound (cyan main chain), ADP bound (blue main chain), and Nt-free structures (green main chain). The side chains of the *cis*-residues are colored as follows: orange for ATP, purple for ADP, and yellow for Nt-free.

(E) The same overlap structures as in (D), except only two side chains of the *cis*-residues (colored as in [D]) at the P loop are drawn.

(F) The overlap of ATP bound (F424 in orange and main chain in cyan) and Nt-free (F424 in yellow and main chain in green) structures of F1-ATPase superimposed on the central β sheet, showing a large movement (11.5 Å) of the F424 loop to pack with the Nt base (in silver) upon ATP binding.

(brown), make direct contact with ATP: tK418 forms three bonds by interacting with γ-Pi, α-Pi, and the oxygen-linking γ-Pi and β-Pi (γ-β oxygen), while tK419 interacts with the ribose. A six *trans*-residue tD499 (gray) does not interact directly with ATP, but it interacts with tR498 as well as with ADP through a water molecule in another structural state (see below) and thus should also be important for ATP/ADP usage by LTag.

"Apical" Water and Its Unusual Coordination in ATP Bound Structure

In the ATP bound structure of LTag, a water molecule W1 is seen at a position apical to the γ-Pi of each of the six ATPs in a hexamer (Figure 5A). In addition, W1 is unusually multiple coordinated by four residues: D474 + N529 from the *cis*-monomer and tR540 + tR498 from the *trans*-monomer. Previously, such apical water was observed to be in the real apical position in structures containing AlF_4^- that mimic the transition state of hydrolyzed γ-Pi (Rittinger et al., 1998; Scheffzek et al., 1997; Tesmer et al., 1997). Here in the ATP bound state (before hydrolysis), W1 not only occupies a near apical position for the nucleophilic attack but also is in a unique multiple bonding geometry that has not been previously described. This bonding geometry is such that tR498 and γ-Pi are on the opposite end of W1, and the other three residues (D474, N529, and tR540) surround W1 from the side, with each of the three residues interacting directly with both the apical W1 and γ-Pi (Figure 5A). The apical waters in each of the six ATP binding sites in a hexamer have essentially the same coordination geometry, and are all in a position ready for the nucleophilic attack on the γ-Pi of ATP for hydrolysis.

"Arginine Finger" versus "Lysine Finger" in ATP Hydrolysis

Unlike other examples of single arginine finger next to the triphosphate to neutralize the developing negative charges in the transition state for ATP hydrolysis (Abrahams et al., 1994; Crampton et al., 2004; Sawaya et al., 1999; Singleton et al., 2000), LTag has three positively charged residues (tR498, tK418, and tR540) supplied in *trans* to interact with the triphosphate of ATP (Figure 5A) either through a water molecule (tR498) or by direct bonding to the phosphate (tK418 and tR540). Residue tR540 interacts with ATP from the end of the triphosphate to contact the γ-Pi and tK418 from the "side" to contact the γ-β oxygen directly (Figure 5A). In this respect, LTag has an unusual lysine finger (tK418) in addition to the canonical arginine finger (tR540) for ATP hydrolysis.

Type I ADP Interactions with *trans*-Residues

Unlike the *cis*-residues around the Nt pocket, the *trans*-residues interacting with the Nt undergo major rearrangements in different Nt binding states (Figures 5A–5E). Even in a ADP bound hexamer, two very different monomer conformations exist. This is manifested by two different types of interactions (type I and II) between the *trans*-residues and the ADP (Figures 5C and 5E). Compared with the ATP state (Figure 5A), tR540 residue in the ADP type I state moves away from the γ-Pi of ATP by 3.6 Å (Figure 5B). Moving in concert with tR540 is tD502, with the original hydrogen bond between the two maintained as they move. Residue tR498 also moves by about 3.7 Å (indicated by the orange arrow in Figure 5B).

In contrast to these gross movements of tR540 and tR498, only subtle changes occur for tK418 (pink side chains) and tK419 (brown side chains) in the transition from ATP state to the ADP type I state (Figure 5B). The ε amino groups of both residues rotate to point in opposite directions, breaking the bonds between tK418 and the phosphate and between tK419 and the pentose (Figures 5A and 5B). Meanwhile, the new orientation of tK418 allows a new bond with tD502 (Figure 5C), which may function to withdraw the ε amino group of tK418 from the phosphate, a subtle change but potentially significant for preparing tK418 to leave the phosphate region and move to the next conformational state (type II state, see below).

Type II ADP Interactions with *trans*-Residues

The type II interactions display a much larger conformational rearrangement of the *trans*-residues when compared with the ATP bound structure (compare Figure 5E to Figure 5A), suggesting that the type II conformation follows type I after ATP hydrolysis. In the transition from type I to type II, tK418 translates along the ADP phosphate and toward the ribose by about 8.3 Å (Figure 5D, the residue in pink), taking the position of tK419 (in brown) that also translates away for a similar distance. The tK418 at the new position makes direct H bonds with the ribose (Figure 5E). There are two other equally dramatic rearrangements involving two pairs of residues: tR540/tD502 and tR498/tD499. Residue tR540, bonding with tD502, moves farther away from the Nt by another 7 Å (Figures 5C–5E). The other pair of residues, tR498/tD499, moves together toward the β-Pi of the ADP by 10.9 Å (Figures 5C–5E). In this new position, tR498 bonds directly to β-Pi, while tD499 bonds to tR498 as well as interacts with the β-Pi through water molecules and Mg^{2+} (Figure 5E). The interactions of tR498/tD499 with the β-Pi here (Figure 5E) are very much like the interactions of tR540/tD502 with the γ-Pi in the ATP bound structure (Figure 5A).

Trans-Residue Conformations in the Absence of Nt

Previously, we have shown that LTag is capable of forming hexamers in the absence of Nt (Li et al., 2003). In the Nt-free structure, the *trans*-residues are farther away from the P loop of the *cis*-monomer than those in the type II ADP state (Figures 5E–5G). This increase in distance between the two neighboring monomers causes a decrease of the interface area in the Nt-free state. In this state, tR498 occupies a position very similar to that of the arginine finger (tR540) in the ATP bound structure (compare Figures 5G and 5A). But upon ATP binding, tR498 clearly swings away to yield the finger position to tR540 and to coordinate the apical water (Figures 5H and 5A).

The Motion of β Hairpins along the Channel

ATP binding/hydrolysis not only changes the domain angles and orientations between D1 and D2/D3, it also affects the conformations of substructures within D2 domain. D2 has a unique β hairpin structure that protrudes into the hexameric channel (Figures 6A and 6B), reminiscent of the six β hairpins in the mtMCM central channel (Fletcher et al., 2003). The β hairpin has several positively charged residues, and mutation of these residues abolishes helicase activity (data not shown), suggesting that these fingers are essential for DNA remodeling activity.

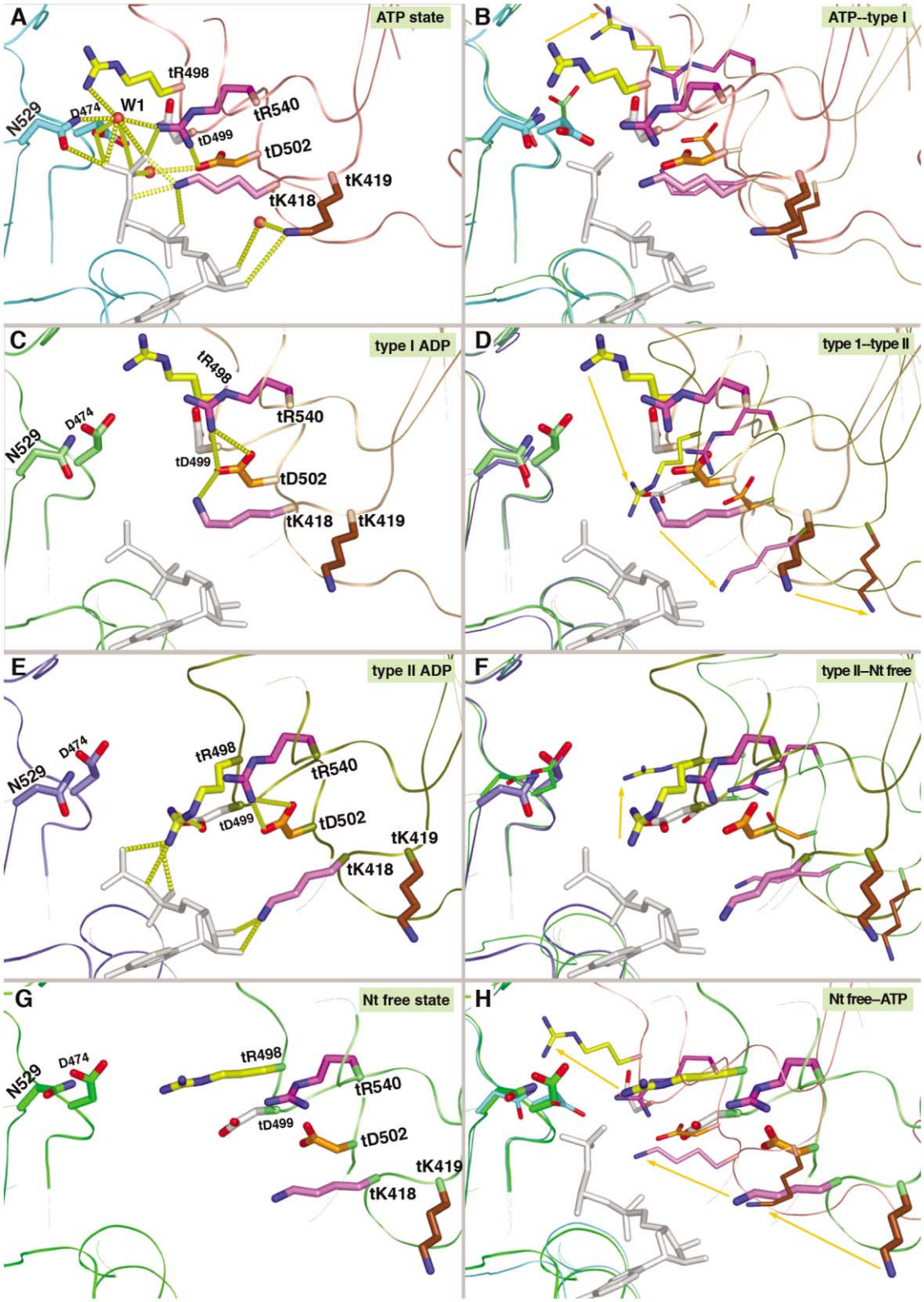

Figure 5. The Conformational Changes of the *trans*-Residues in Response to ATP Binding, Hydrolysis, and ADP Release

All the structural overlaps were based on the superposition of the D2 β sheet of the *cis*-monomer. (A) Positions of the *trans*-residues and their interactions with ATP bound to the *cis*-monomer. The six *trans*-residues (with a "t-" in front) are drawn in different color. Two *cis*-residues on the left side (D474 and N529, in cyan) are shown. Dashed lines denote hydrogen bonds. (B) The overlap of the ATP bound structure (with thicker side chains, as in [A]) and ADP bound (with thinner side chains) structure (as in [C]). The *trans*-residue shifts correlate to the

Indeed, the β hairpin conformation and position change dramatically in response to ATP binding, hydrolysis, and ADP release, resulting in movements along the central channel in large steps, with an ~17 Å move toward D1 direction upon ATP binding (step 1 in Figure 6C), an ~6.7 Å move to type I ADP state following ATP hydrolysis (step 2 in Figure 6D), an ~6.6 Å move to type II from type I ADP state (step 3 in Figure 6D), and an ~6.2 Å move upon ADP release (step 4 in Figure 6D). These movements are due to the changes in the orientations between D2/D3 and D1 as well as in the β hairpin structure itself. Three of the six *trans*-residues responding to Nt binding (tR498, tD499, and tD502, Figure 6E) are located right at the base (N-terminal end) of the β hairpin, providing an efficient lever for modulating its conformation and movement along the central channel. The other three residues (tK418, tK419, and tR540) locate on one end of β strand S1 and S5. The other ends of strands S1 and S5 contact the Nt on the next interface (Figures 6E and 6F), providing another kind of "mechanical" connection between two neighboring sites for conformational changes.

Discussion

We describe a set of structures of LTag corresponding to ATP (and ADP-BeF_3^-+Mg^{2+}), ADP, and Nt-free states. These structures support an all-or-none Nt binding mode and a concerted ATP hydrolysis mechanism. They also reveal the detailed molecular mechanisms of ATP binding and hydrolysis by this hexameric helicase. Furthermore, they elucidate the detailed mechanisms of conformational changes triggered by ATP binding and hydrolysis, which are proposed to be coupled to DNA translocation and unwinding.

An All-or-None Binding Mode

Among the hexameric molecular machines that use NTP, available evidence supports a sequential (or rotary) NTP binding and hydrolysis mechanism. For example, the F1-ATPase hexamer has three active ATPase sites, but only two are occupied at a given time, one by ATP and the other by ADP+Pi (Abrahams et al., 1994; Menz et al., 2001). This partial occupancy by a mixture of ATP and ADP is not affected by Nt concentration (Abrahams et al., 1994; Menz et al., 2001). The hexamers of T7 gp4 and Rho have six active NTPase sites (Hingorani et al., 1997; Stitt and Xu, 1998), but only four may be occupied at a given moment, two with NTP and two with NDP+Pi (Kim et al., 1999; Singleton et al., 2000). Despite the difference in the number of occupied sites, both systems share a common mechanism of sequential NTP binding and hydrolysis (Leslie et al., 1999; Singleton et al., 2000; Stock et al., 1999).

However, the structural data of LTag described here suggest a different Nt binding and hydrolysis mechanism. The following evidence supports an all-or-none Nt binding mode. First, various Nt concentrations and combinations were used for cocrystallization with LTag in order to obtain the structures with partial occupancy of ATP, ADP, or a mixture of ATP and ADP. However, the many structures of LTag hexamer determined so far are either completely Nt-free (in P321 and P6 space groups at 3.8 Å, data not shown) or completely occupied with a single type of Nt (in C2 and R3). This result is consistent with a previous kinetic study showing a 1:1 ratio of ATP or ADP to LTag (monomer) in solution (Huang et al., 1998). Second, the structures containing either ATP or ATP analog (ADP-BeF_3^-) were obtained differently, one by cocrystallization and the other by soaking. Nonetheless, both structures are fully occupied with ATP or ATP analog. Third, the crystal soaked with ATP-BeF_3^- or ADP-BeF_3^- underwent a transformation from C2 (ADP bound form) to $P2_1$ (ATP mimic form) space group. We found that the structure transformation was an all or none process, and no intermediate form was obtained despite extensive experimenting with various conditions. Once the transformation occurs, it always produces a hexamer structure with a full occupancy by the ATP analog. These structural data represent the first clear-cut example of an all-or-none (or concerted) Nt binding mode for a hexameric helicase or an AAA^+ molecular machine.

Concerted ATP Hydrolysis

The all-or-none ATP or ADP binding mode would be compatible with a concerted (or synchronized) ATP hydrolysis mechanism, which is also supported by two additional features observed in the structure containing ADP-BeF_3^-+Mg^{2+}, an ATP+Mg^{2+} analog. First, the unique apical water is present in all six ATP sites in a hexamer (Figure 5A). Moreover, all six apical waters have essentially the same multiple coordination geometry and are all in a position ready for the nucleophilic attack on the γ-Pi of ATP for simultaneous hydrolysis. Second, the two unusual fingers for ATP hydrolysis, the arginine finger (tR540) and lysine finger (tK418) (Figure 5A), are positioned almost identically next to the triphosphate in all six ATP sites, possibly for synchronized hydrolysis. The presence of two distinct conformations of the ADP bound structure appears to contradict a concerted hydrolysis mechanism. Nonetheless, it may simply reflect the need to break symmetry of the hexamer for DNA unwinding after concerted ATP hydrolysis. The observation that only completely Nt-free or fully ADP-occupied structures were obtained suggests that the ADP release may also be concerted.

conformational changes upon ATP hydrolysis. The arrow in orange indicates the shift of tR498. (C) Positions of the *trans*-residues and their interactions with ADP in the type I state. (D) The overlap of two types of ADP bound conformations (type I and type II). The structure with thicker side chains represents type I, as shown in (C), and the structure with thinner side chains is the type II as shown in (E). The arrows in orange indicate shifts of the *trans*-residues from type I to type II. (E) Positions of the *trans*-residues and their interactions with ADP in type II state. (F) The overlap of type II ADP bound structure (with thicker side chains, as in [E]) with the Nt-free structure (with thinner side chains). (G) Positions of the *trans*-residues in the Nt-free structure. (H) The overlap of Nt-free structure (with thicker side chains) with ATP bound structure (with thinner side chains).

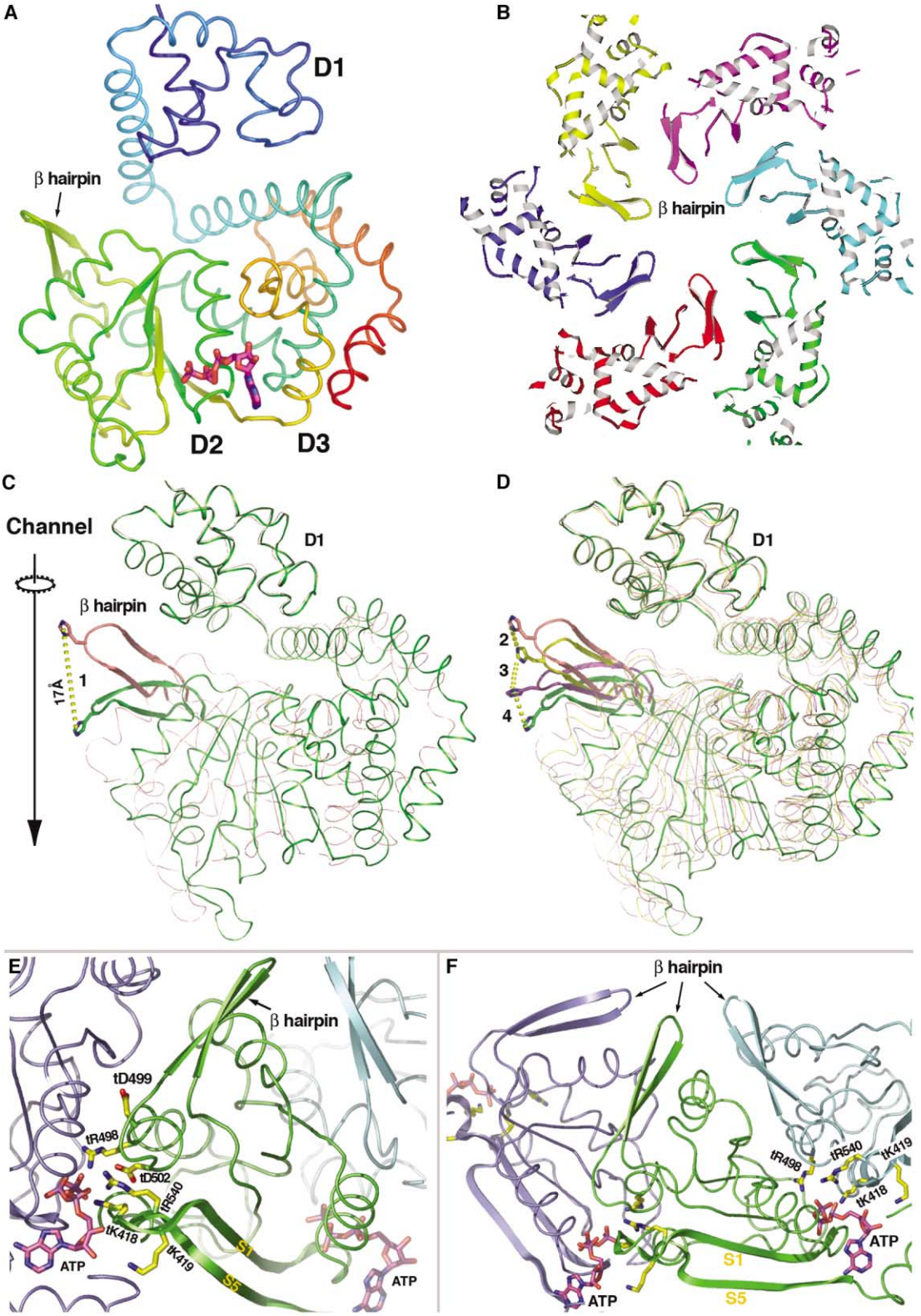

Figure 6. The β Hairpin Structures and Their Movement

(A) The ATP binding site in D2/D3 of a LTag monomer, showing that D1 is well-separated from the ATP site (ATP in red).

(B) The six β hairpins (residues 508–517) in the central channel, viewing along the hexameric channel axis.

(C) Overlap of LTag monomer structures between the Nt-free structure (green) and the ATP bound structure (pink), based on the superposition of D1. The yellow dash line shows the moving distance of the β hairpin upon ATP binding.

(D) The same overlap as in (C), with the addition of two ADP bound conformational states (yellow and purple). The yellow dash lines indicate the moving steps of the β hairpin in different Nt states.

Double Fingers for ATP Hydrolysis

Some NTP-hydrolyzing systems use an arginine finger for hydrolysis (Wittinghofer, 1998). How the arginine is positioned next to the triphosphate of ATP determines whether the hydrolysis mechanism is associative or dissociative (Maegley et al., 1996). If the mechanism is associative, in which partial negative charge develops in the γ-Pi in the transition state, the arginine finger interacts with the γ-Pi from the end to neutralize the developing charges, catalyzing hydrolysis. If it is dissociative, in which the developing charges concentrate on the γ-β oxygen, the arginine finger focuses its interactions with the γ-β oxygen from the side. In this regard, LTag is unique in that it has two fingers (an arginine and a lysine finger), one positioned next to the end and the other to the side of the triphosphate (Figure 5A). This distribution of the arginine and lysine fingers may suggest a combination of dissociative and associative mechanisms for ATP hydrolysis.

Conformation Change: Not a *cis*-Effect

An important question is how ATP binding/hydrolysis triggers the large conformational change in LTag, as shown in Figures 2 and 3. It is apparent that LTag Nt binding pocket is somewhat detached from the N-terminal D1 (Figure 6A), suggesting that Nt binding should not affect the domain orientation of the same monomer (*cis*-monomer). Moreover, lack of structural changes of the *cis*-residues around the Nt pocket in different Nt binding states (Figure 4D) suggests that the large changes of domain orientation (Figure 3) could not originate from the Nt pocket of the same monomer (not a *cis*-effect). This is different from the known mechanisms in other systems (such as F1-ATPase [Walker, 1994] and the Ras-GTPase Ras-GTPase [Scheffzek et al., 1997]) where ATP binding/hydrolysis at the interface between two molecules triggers significant conformational changes around the Nt pocket in the same monomer (*cis*-effect). For example, in the hexameric F1-ATPase, ATP binding triggers closure of a gap at the Nt pocket of the *cis*-monomer (Figure 4F), causing a large conformational change of a distal domain in the *cis*-monomer (Walker, 1994). Thus, the absence of a *cis*-effect for the conformational changes triggered by ATP binding in LTag is distinctive and may be a general feature for other AAA^+ hexameric molecular machines.

Conformation Change via *trans*-Effect

The *trans*-residues that interact with the Nt bound to the *cis*-monomer undergo large structural rearrangement in response to ATP binding, hydrolysis, and ADP release. It is the structural arrangement of these *trans*-residues that leads to an overall orientation change between domains of the *trans*-monomer (*trans*-effect). When ATP binds to the *cis*-monomer, the *trans*-residues tR540, tD502, tK418, and tK419 move toward the ATP site to interact with the ATP (Figures 5H and 5A), pulling D2/D3 of the *trans*-monomer closer to the *cis*-monomer (Figure 2E). Because this pulling occurs only at D2/D3 and not at the N-terminal D1, the net effect is the change of angle and orientation of D2/D3 relative to D1 in the *trans*-monomer, generating closure and twist between the N- and C-terminal domains in response to ATP binding (Figures 3B and 3E).

Similarly, hydrolysis of ATP to ADP results in further rearrangement of the *trans*-residues at the interface. In particular, from the ATP to the ADP state, the pair tR540/tD502 moves away from the Nt phosphate (Figures 5A, 5C, and 5E), while the pair tR498/tD499 rearranges to establish direct contact with the ADP phosphate, in two discernable steps (type I and type II states). Also in two steps, tK418 first breaks the bonds with the Nt phosphate through a subtle conformational change (Figures 5A–5C) and then translates a long distance to interact with the pentose (Figures 5C–5E). As these *trans*-residues change their positions relative to the Nt bound to the *cis*-monomer, they force D2/D3 of the *trans*-monomer to move with them, generating new angles and orientations between D2/D3 and D1 in each step (Figures 3C and 3F).

It is through this *trans*-effect (i.e., through the responsiveness of the *trans*-residues) in the context of a hexamer that domain closure and twist are achieved by ATP binding and hydrolysis. The domain closure and twist of a monomer led to two apparent conformational changes in the hexamer: (1) producing the net effect of twisting/untwisting between the two layers of the hexamer ring (composed of D1 and D2/D3, respectively), and (2) causing the expansion and constriction of the hexameric channel, a motion similar to what is described in the iris model (Li et al., 2003). These two conformational changes are likely coupled to origin melting and DNA unwinding during helicase action.

Finger, Sensor, and Lever

In the process of conformational changes triggered by ATP binding, hydrolysis, and ADP release, three positively charged *trans*-residues—tR540 (arginine finger), tK418 (lysine finger), and tR498—have two distinct but essential roles: (1) they participate in ATP hydrolysis by serving as the fingers (tR540 and tK418) and by coordinating the apical water, and (2) they provide mechanical leverage for conformational changes by sensing the presence and coordinating the binding of ATP and ADP. Residues tR540 and tR498 each bond with a negatively charged residue (tR540 with tD502, tR498 with tD499), and the paired residues always move in concert during the conformational changes in response to ATP binding and hydrolysis, suggesting that these two negatively charged residues may also play an important role in helicase function.

(E) The sensor and lever roles of the *trans*-residues. Residues tR498, tD499, and tD502 are located at the base (N-terminal end) of the β hairpin. Residues tK418, tK419, and tR540 are at one end of β strands S1 and S5 that uses the other ends to interact with an Nt in the next interface.

(F) The mechanical connection between two adjacent Nt binding sites through strands S1 and S5. The four *trans*-residues (tK418, tK419, tR495, and tR540) interacting with the Nt are drawn. These *trans*-residues not only sense the presence of Nt through direct contact but also provide a mechanical leverage for changing the conformations of the *trans*-monomer in response to ATP binding, hydrolysis, and ADP release.

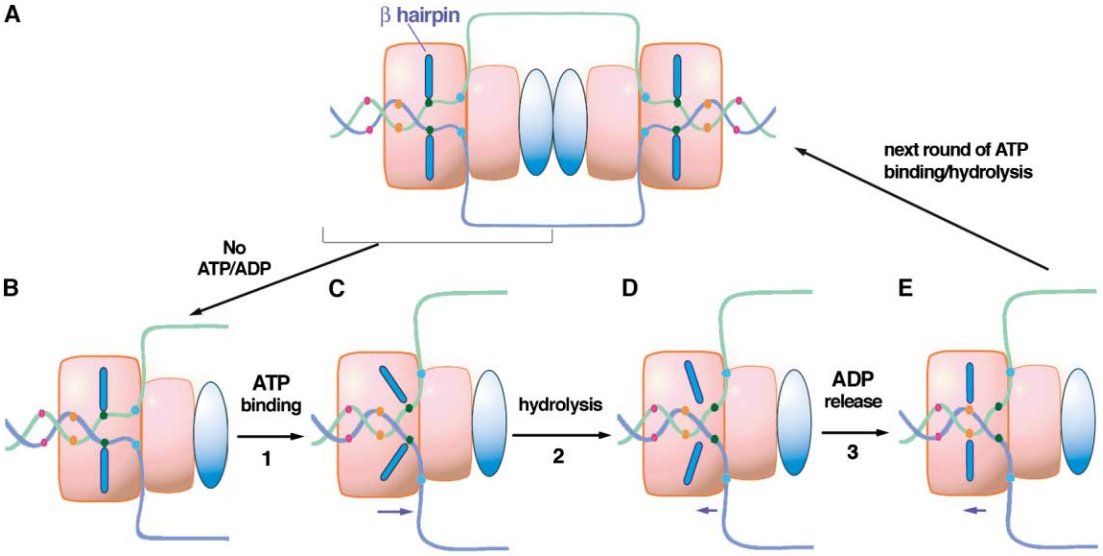

Figure 7. A Looping Model Showing the Coupling of the β Hairpin Movement to the dsDNA Translocation into LTag Double Hexamer for Unwinding

The β hairpins move along the central channel in response to ATP binding (step 1), hydrolysis (step 2), and ADP release (step 3). (A) LTag double hexamer with two ssDNA loops coming out from the side channels. Each hexamer contains a helicase domain (represented by two squares in pink) and an OBD (oval in light blue). The β hairpin structure is represented by two bars (in blue) within the helicase domain. The colored dots on the DNA (red, orange, black, and blue) are position markers for translocation. (B) A LTag hexamer corresponding to the left half of the double hexamer in (A) in the Nt-free state. (C) The movement of β hairpins upon ATP binding, which serves to pull dsDNA into the helicase for unwinding. The unwound ssDNA extrudes from the side channels. For clarity, only one hexamer is shown. (D) The β hairpins move back about halfway toward the Nt-free position after ATP hydrolysis. (E) The ADP is released from the LTag hexamer, and the β hairpins return to the original Nt-free position.

Coupling ATP Binding/Hydrolysis to DNA Translocation/Unwinding

Based on the observations in this report, we have refined our previous looping model (Li et al., 2003) for bidirectional fork unwinding (Figure 7). First, an alternative conformation is proposed for the ssDNA loops coming out from the double hexamer, i.e., each end of a ssDNA loop exiting through a side channel of a helicase domain on both ends of the double hexamer (Figure 7A). Second, during bidirectional fork unwinding, the movement of the β hairpins in the central channel is coupled to the translocation of dsDNA into the double hexamer for unwinding (Figures 7B–7E). In the Nt-free state, the β hairpin structure is in a "relaxed" state (Figures 7A and 7B). When LTag binds ATP, the β hairpins move toward the N-terminal D1 (the center of the double hexamer) by about 17 Å (Figures 7C and 6C), pulling/pushing the dsDNA into the double hexamer by about 5–6 bp (~3.2–3.4 Å/bp for B-DNA), promoting strand separation and propelling ssDNA extrusion from the side channel (Figure 7C). Third, ATP hydrolysis to ADP triggers further conformational changes, causing the hairpins to move toward its original Nt-free position (Figure 7D). Fourth, ADP release from the hexamer results in a complete relaxation of the β hairpin structure to the original Nt-free position (Figure 7E), setting a stage for the next cycle of ATP binding and hydrolysis during DNA unwinding.

In summary, we have described several structures of LTag in different Nt binding states. These structures provide detailed information regarding the conformational changes of a hexameric machine in response to Nt binding, hydrolysis, and release. The data presented here support an all-or-none Nt binding mode and a concerted ATP hydrolysis mechanism, which is different from the rotary (or sequential) mechanism for other known hexameric machines. Furthermore, the conformational changes of LTag provide a mechanism for coupling the energy of ATP binding and hydrolysis to DNA translocation and unwinding in DNA replication. Mechanisms described here for LTag may be applicable to some other hexameric molecular machines, including helicases and AAA^+ proteins.

Experimental Procedures

Protein Expression, Purification, and Crystallization

LTag251–627 was produced using *E. coli* expression system as previously described (Li et al., 2003). Briefly, the protein was expressed as a GST-LTag fusion using the pGEX-2T vector, with a thrombin cleavage site between GST and LTag. The fusion protein was first purified by glutathione affinity column. The GST was released by thrombin cleavage, and the LTag fragment was further purified by ion exchange and Superdex 200 gel filtration chromatography. The protein was concentrated to 20 mg/ml in a buffer containing 25 mM Tris-Cl (pH 8.0), 250 mM NaCl, and 10 mM DTT. Crystals were grown at 4°C by hanging drop vapor diffusion method. The P321 crystal form (a = b = 120.3 Å, c = 132.4 Å) was grown in the absence of Nt. The C2 (ADP bound) form (a = 196.3 Å, b = 86.6 Å, c = 129.7 Å, β = 129.2°) was obtained in the presence of either ATP+$MgSO_4$ or ADP+$MgSO_4$. The ADP-BeF_3^- bound form was obtained by soaking ADP bound C2 crystals with a mixture of BeF_3^- (2 mM), $MgSO_4$ (0.05 M), and ADP (or ATP). Soaking with either ADP+BeF_3^- or ATP+BeF_3^- resulted in a transformation from C2 space group to $P2_1$ (a = 125.4 Å, b = 89.2 Å, c = 149.5 Å, β = 91.3°), and the two soaks yielded essentially the same structure. The ATP bound crystal form was grown in the presence of ATP but

in the absence Mg^{2+}, a condition not allowing ATP hydrolysis. The space group is R3 (a = b = 170.3 Å, c = 128.7 Å).

Data Collection, Structure Determination, and Refinement

Data sets were collected at the APS 19ID (SBC) and 14BMC (BioCARS) beamlines, Argonne National Laboratory. Crystals were flash frozen in liquid nitrogen in crystallization buffer supplemented with 25% glycerol. Data were processed with HKL2000 (Otwinowski and Minor, 1997) (Table 1). The structures of LTag in different crystal forms were determined by molecular replacement (MR) using the CNS program suite. The search model for MR was the D2/D3 domains (residues 355–627) of the Nt-free structure of LTag (Li et al., 2003). Because of the domain angle changes of LTag monomers, using the whole helicase domain (D1+D2/D3) as the search model did not generate obvious solutions. After obtaining the solutions from MR, a rigid body refinement was carried out using CNS (Brunger et al., 2001), followed by simulated annealing at 6000 K. A final B-individual refinement was carried out before Fourier difference map calculation to reveal the presence of Nts, and further refinements were performed after adding the Nt to yield the full refinement statistics (Table 1). No noncrystallographic (ncs) averaging or ncs constraints/restraints were used in any of the refinement steps.

Acknowledgments

We thank L.G. Chen for her assistance in preparing figures; Drs. R. Garcea, L. Chen, M. Churchill, and J. Kieft for comments on the manuscript; other members of the X. Chen lab for help and input; staff at the APS 19id (SBC) and 14bmc (BioCARS) beamlines in Argonne Natl. Lab for assistance in data collection; and the UCHSC X-Ray Centre for support. This work is supported in part by a fellowship from the Colorado Cancer League to D.G., a fellowship from AHA to C.V.F., and NIH-R01 to X.S.C.

Received: April 16, 2004
Revised: September 3, 2004
Accepted: September 3, 2004
Published: September 30, 2004

References

Abrahams, J.P., Leslie, A.G., Lutter, R., and Walker, J.E. (1994). Structure at 2.8 Å resolution of F1-ATPase from bovine heart mitochondria. Nature *370*, 621–628.

Arthur, A.K., Hoss, A., and Fanning, E. (1988). Expression of simian virus 40 T antigen in *Escherichia coli*: localization of T-antigen origin DNA-binding domain to within 129 amino acids. J. Virol. *62*, 1999–2006.

Borowiec, J.A., Dean, F.B., Bullock, P.A., and Hurwitz, J. (1990). Binding and unwinding—how T antigen engages the SV40 origin of DNA replication. Cell *60*, 181–184.

Borowiec, J.A., Dean, F.B., and Hurwitz, J. (1991). Differential induction of structural changes in the simian virus 40 origin of replication by T antigen. J. Virol. *65*, 1228–1235.

Brunger, A.T., Adams, P.D., Clore, G.M., Delano, W.L., Gros, P., Grosse-Kunstleve, R.W., Jiang, J.-S., Kuszewski, J., Nilges, M., Pannu, N.S., et al. (1998). Crystallography and NMR system (http://cns.csb.yale.edu).

Brush, G.S., Kelly, T.J., and Stillman, B. (1995). Identification of eukaryotic DNA replication proteins using simian virus 40 in vitro replication system. Methods Enzymol. *262*, 522–548.

Bullock, P.A. (1997). The initiation of simian virus 40 DNA replication in vitro. Crit. Rev. Biochem. Mol. Biol. *32*, 503–568.

Bullock, P.A., Seo, Y.S., and Hurwitz, J. (1991). Initiation of simian virus 40 DNA synthesis in vitro. Mol. Cell. Biol. *11*, 2350–2361.

Campbell, K.S., Mullane, K.P., Aksoy, I.A., Stubdal, H., Zalvide, J., Pipas, J.M., Silver, P.A., Roberts, T.M., Schaffhausen, B.S., and DeCaprio, J.A. (1997). DnaJ/hsp40 chaperone domain of SV40 large T antigen promotes efficient viral DNA replication. Genes Dev. *11*, 1098–1110.

Chong, J.P., Hayashi, M.K., Simon, M.N., Xu, R.M., and Stillman, B. (2000). A double-hexamer archaeal minichromosome maintenance protein is an ATP-dependent DNA helicase. Proc. Natl. Acad. Sci. USA *97*, 1530–1535.

Crampton, D.J., Guo, S., Johnson, D.E., and Richardson, C.C. (2004). The arginine finger of bacteriophage T7 gene 4 helicase: role in energy coupling. Proc. Natl. Acad. Sci. USA *101*, 4373–4378.

Dean, F.B., Bullock, P., Murakami, Y., Wobbe, C.R., Weissbach, L., and Hurwitz, J. (1987). Simian virus 40 (SV40) DNA replication: SV40 large T antigen unwinds DNA containing the SV40 origin of replication. Proc. Natl. Acad. Sci. USA *84*, 16–20.

Fanning, E., and Knippers, R. (1992). Structure and function of simian virus 40 large tumor antigen. Annu. Rev. Biochem. *61*, 55–85.

Fisher, A.J., Smith, C.A., Thoden, J.B., Smith, R., Sutoh, K., Holden, H.M., and Rayment, I. (1995). X-ray structures of the myosin motor domain of Dictyostelium discoideum complexed with MgADP.BeFx and MgADP.AlF4−. Biochemistry *34*, 8960–8972.

Fletcher, R., Bishop, B., Sclafani, R., Leon, R., Ogata, G., and Chen, X. (2003). The structure and function of MCM dodecamer from archaeal M. Thermoautotrophicum. Nat. Struct. Biol. *10*, 160–167.

Gomez-Lorenzo, M.G., Valle, M., Frank, J., Gruss, C., Sorzano, C.O., Chen, X.S., Donate, L.E., and Carazo, J.M. (2003). Large T antigen on the simian virus 40 origin of replication: a 3D snapshot prior to DNA replication. EMBO J. *22*, 6205–6213.

Hingorani, M.M., Washington, M.T., Moore, K.C., and Patel, S.S. (1997). The dTTPase mechanism of T7 DNA helicase resembles the binding change mechanism of the F1-ATPase. Proc. Natl. Acad. Sci. USA *94*, 5012–5017.

Huang, S.G., Weisshart, K., and Fanning, E. (1998). Characterization of the nucleotide binding properties of SV40 T antigen using fluorescent 3′(2′)-O-(2,4,6-trinitrophenyl)adenine nucleotide analogues. Biochemistry *37*, 15336–15344.

Kelman, Z., Lee, J.K., and Hurwitz, J. (1999). The single minichromosome maintenance protein of Methanobacterium thermoautotrophicum DeltaH contains DNA helicase activity. Proc. Natl. Acad. Sci. USA *96*, 14783–14788.

Kim, D.E., Shigesada, K., and Patel, S.S. (1999). Transcription termination factor Rho contains three noncatalytic nucleotide binding sites. J. Biol. Chem. *274*, 11623–11628.

Leslie, A.G., Abrahams, J.P., Braig, K., Lutter, R., Menz, R.I., Orriss, G.L., van Raaij, M.J., and Walker, J.E. (1999). The structure of bovine mitochondrial F1-ATPase: an example of rotary catalysis. Biochem. Soc. Trans. *27*, 37–42.

Levin, M.K., Gurjar, M.M., and Patel, S.S. (2003). ATP binding modulates the nucleic acid affinity of hepatitis C virus helicase. J. Biol. Chem. *278*, 23311–23316. Published online March *26*, 2003.

Li, D., Zhao, R., Lilyestrom, W., Gai, D., Zhang, R., DeCaprio, J.A., Fanning, E., Jochimiak, A., Szakonyi, G., and Chen, X.S. (2003). The structure of the replicative helicase of the oncoprotein SV40 large tumour antigen. Nature *423*, 512–518.

Maegley, K.A., Admiraal, S.J., and Herschlag, D. (1996). Ras-catalyzed hydrolysis of GTP: a new perspective from model studies. Proc. Natl. Acad. Sci. USA *93*, 8160–8166.

Menz, R.I., Leslie, A.G., and Walker, J.E. (2001). The structure and nucleotide occupancy of bovine mitochondrial F(1)-ATPase are not influenced by crystallisation at high concentrations of nucleotide. FEBS Lett. *494*, 11–14.

Neuwald, A.F., Aravind, L., Spouge, J.L., and Koonin, E.V. (1999). AAA+: a class of chaperone-like ATPases associated with the assembly, operation, and disassembly of protein complexes. Genome Res. *9*, 27–43.

Ogura, T., and Wilkinson, A.J. (2001). AAA+ superfamily ATPases: common structure—diverse function. Genes Cells *6*, 575–597.

Otwinowski, Z., and Minor, W. (1997). Processing of X-ray diffraction data collected in oscillation mode. Methods Enzymol. Macromolecular Crystallography A *276*, 307–326.

Petsko, G.A. (2000). Chemistry and biology. Proc. Natl. Acad. Sci. USA *97*, 538–540.

Rittinger, K., Taylor, W.R., Smerdon, S.J., and Gamblin, S.J. (1998). Support for shared ancestry of GAPs. Nature *392*, 448–449.

Sawaya, M.R., Guo, S., Tabor, S., Richardson, C.C., and Ellenberger, T. (1999). Crystal structure of the helicase domain from the replicative helicase-primase of bacteriophage T7. Cell *99*, 167–177.

Scheffzek, K., Ahmadian, M.R., Kabsch, W., Wiesmuller, L., Lautwein, A., Schmitz, F., and Wittinghofer, A. (1997). The Ras-RasGAP complex: structural basis for GTPase activation and its loss in oncogenic Ras mutants. Science *277*, 333–338.

Simmons, D.T. (2000). SV40 large T antigen functions in DNA replication and transformation. Adv. Virus Res. *55*, 75–134.

Singleton, M.R., Sawaya, M.R., Ellenberger, T., and Wigley, D.B. (2000). Crystal structure of T7 gene 4 ring helicase indicates a mechanism for sequential hydrolysis of nucleotides. Cell *101*, 589–600.

Smelkova, N.V., and Borowiec, J.A. (1998). Synthetic DNA replication bubbles bound and unwound with twofold symmetry by a simian virus 40 T-antigen double hexamer. J. Virol. *72*, 8676–8681.

Stillman, B. (1994). Smart machines at the DNA replication fork. Cell *78*, 725–728.

Stillman, B.W., and Gluzman, Y. (1985). Replication and supercoiling of simian virus 40 DNA in cell extracts from human cells. Mol. Cell. Biol. *5*, 2051–2060.

Stillman, B., Gerard, R.D., Guggenheimer, R.A., and Gluzman, Y. (1985). T antigen and template requirements for SV40 DNA replication in vitro. EMBO J. *4*, 2933–2939.

Stitt, B.L., and Xu, Y. (1998). Sequential hydrolysis of ATP molecules bound in interacting catalytic sites of Escherichia coli transcription termination protein Rho. J. Biol. Chem. *273*, 26477–26486.

Stock, D., Leslie, A.G., and Walker, J.E. (1999). Molecular architecture of the rotary motor in ATP synthase. Science *286*, 1700–1705.

Sullivan, C.S., and Pipas, J.M. (2002). T antigens of simian virus 40: molecular chaperones for viral replication and tumorigenesis. Microbiol. Mol. Biol. Rev. *66*, 179–202.

Tesmer, J.J., Sunahara, R.K., Gilman, A.G., and Sprang, S.R. (1997). Crystal structure of the catalytic domains of adenylyl cyclase in a complex with Gsalpha.GTPgammaS. Science *278*, 1907–1916.

Tsurimoto, T., and Stillman, B. (1991). Replication factors required for SV40 DNA replication in vitro. I. DNA structure-specific recognition of a primer-template junction by eukaryotic DNA polymerases and their accessory proteins. J. Biol. Chem. *266*, 1950–1960.

Waga, S., and Stillman, B. (1994). Anatomy of a DNA replication fork revealed by reconstitution of SV40 DNA replication in vitro. Nature *369*, 207–212.

Walker, J.E. (1994). The regulation of catalysis in ATP synthase. Curr. Opin. Struct. Biol. *4*, 912–918.

Wessel, R., Schweizer, J., and Stahl, H. (1992). Simian virus 40 T-antigen DNA helicase is a hexamer which forms a binary complex during bidirectional unwinding from the viral origin of DNA replication. J. Virol. *66*, 804–815.

Wittinghofer, A. (1998). Signal transduction via Ras. Biol. Chem. *379*, 933–937.

Wobbe, C.R., Weissbach, L., Borowiec, J.A., Dean, F.B., Murakami, Y., Bullock, P., and Hurwitz, J. (1987). Replication of simian virus 40 origin-containing DNA in vitro with purified proteins. Proc. Natl. Acad. Sci. USA *84*, 1834–1838.

Accession Numbers

The ATP bound, ADP bound, and Nt-free structures of LTag have been deposited into the Protein Data Bank under ID codes 1SVM, 1SVL, and 1SVO, respectively.